STUDIES OF RV TAURI STARS. I. U MONOCEROTIS*

HELMUT A. ABT†
Lick Observatory, University of California
Received December 20, 1954

ABSTRACT

High-dispersion spectrograms of the low-velocity RV Tauri star U Monocerotis have been obtained regularly for $6\frac{1}{2}$ months, or for more than four light-minima. The results from these plates are compared with a few photoelectric observations and an A.A V S O. light-curve. The spectrograms show that the radial-velocity-curve has a discontinuity at each light-maximum Displacements of the atmosphere, computed from the radial-velocity-curve, are as large as 55×10^6 km; they are large during cycles of deep light-minima and small during cycles of shallow minima Curves of growth have been constructed from line intensities on 17 spectrograms, including some with double absorption lines. Large apparent abundance changes during times of single lines are attributed to a variable continuous opacity within the regions of line formation Ionization temperatures computed with numerical values of the variable continuous opacity are probably in agreement with other determinations of the temperature. Within their probable errors, the rates of change of ionization temperature and of electron pressure with displacement are independent of cycle or direction of motion.

I. INTRODUCTION

This, the first of a series of papers on RV Tauri stars, is concerned with U Monocerotis; other papers will deal with R Scuti and AC Herculis. All three of these stars are members of the low-velocity group of RV Tauri stars (Joy 1952), but it will be seen that in the behavior of their atmospheres these stars more closely resemble W Virginis than the classical Cepheids. The principal observations of U Monocerotis discussed are high-dispersion spectrograms taken at the Lick Observatory at an average interval of 10 days for $6\frac{1}{2}$ months. In addition, a few photoelectric observations in two colors and a visual light-curve from the A.A.V.S.O. are given.

In this paper we attempt to locate the regions of formation of the absorption lines and to obtain some information about the nature of these regions from a study of line intensities. The analysis generally follows standard methods for normal stars. If it should eventually be shown that this star is so abnormal in certain respects that these methods should not have been applied, the corresponding results must be disregarded.

II. PHOTOMETRIC OBSERVATIONS

The A.A.V.S.O. visual light-curve of U Monocerotis for the winter of 1952–1953 (when the spectra were being obtained) was provided by Mrs. M. W. Mayall from observations made principally by Messrs. Yamada, of Japan, and Elias, of Greece. The curve (Fig. 1) shows, successively, a deep light-minimum, a shallow one, two moderate ones, and part of a deep one.

A few photoelectric observations were obtained by O. J. Eggen and by the author, as shown in Table 1. Eggen's observations were obtained with a 1P21 photomultiplier and the Lick 12-inch refractor; his magnitudes and colors have been converted to the ***P***, ***V*** system (Eggen 1951*b*). The author's measures were obtained with an E.M.I. photomultiplier and the 12-inch refractor. A conversion to the ***P***, ***V*** system was made from observations of the Harvard C-12 region on two nights. On most of the nights a comparison was made simply with the neighboring stars HD 59692 ($V = 7.53$, $P - V = -0.03$)

* *Contributions from the Lick Observatory*, Ser II, No. 57.

† Now at the Yerkes and McDonald Observatories.

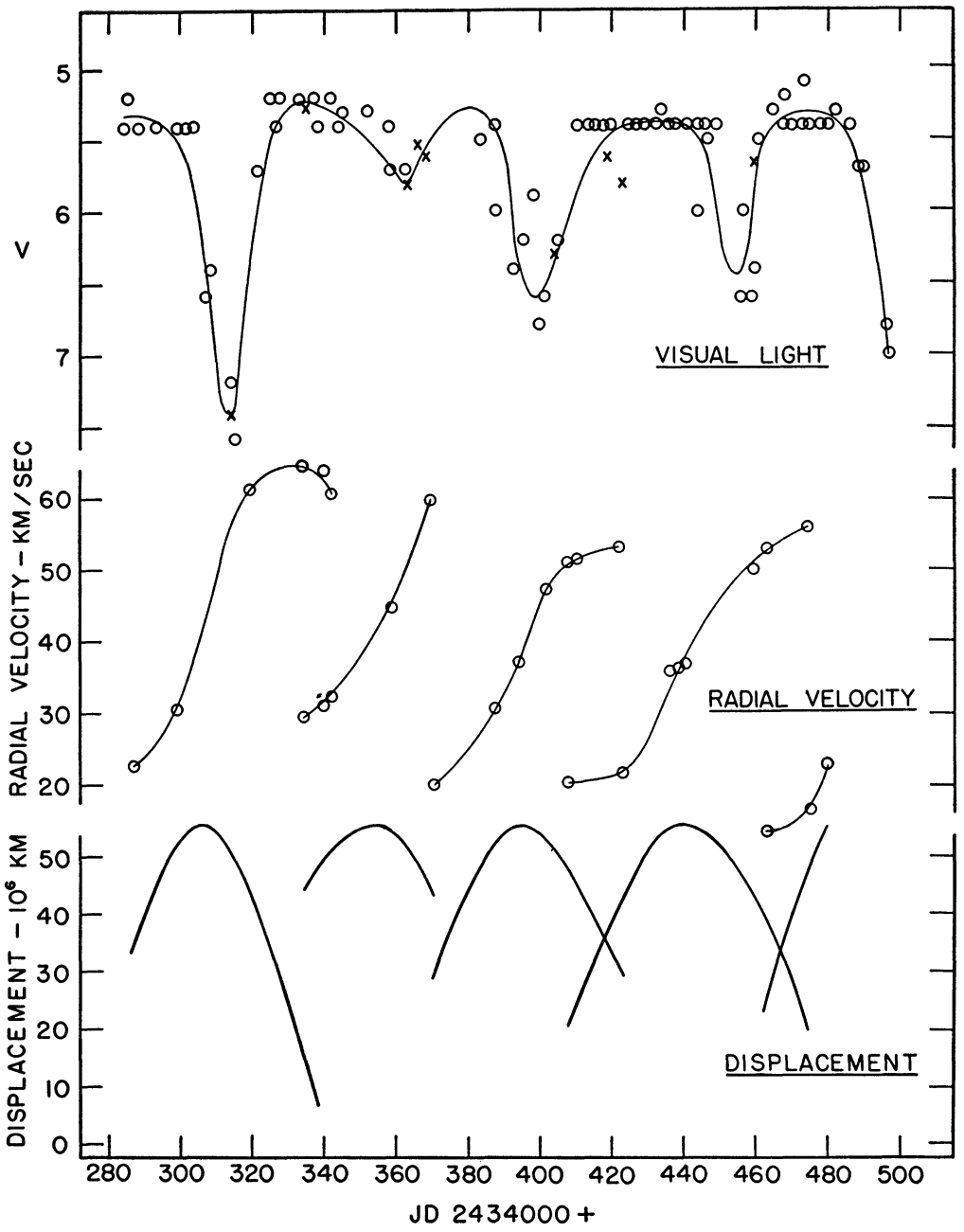

FIG. 1.—*Top:* photoelectric (*crosses*) and A.A.V.S.O. (*circles*) visual magnitudes. The latter were adjusted to the former by a scale correction. *Center:* radial-velocity measures *Bottom:* displacements, $r - r_n$, from unknown zero points, r_n, for each cycle, n, computed from the radial-velocity-curve without assuming a limb-darkening correction factor. For purposes of this illustration we have set all the maximum displacements equal.

and HD 59730 ($V = 6.44$, $P - V = +1.56$). The photoelectric observations are given in the first three columns of Table 1.

A comparison of the photoelectric visual light-observations with those by the A.A.V.S.O. shows the latter to be systematically fainter near light-maxima but in agreement at $V = 7.4$. This difference is probably due to the assumed magnitudes of the brighter comparison stars used by the A.A.V.S.O. A correlation between the two scales was found, and the A.A.V.S.O. values were adjusted accordingly. All observations are plotted in Figure 1. In the case of a large discrepancy between the few photoelectric observations (e.g., JD 2434419 and 2434424) and the many visual estimates, the proper weighting of the two determinations is unknown.

The colors show very little correlation with light; the star is often as blue during a light-minimum as during a maximum, or even bluer. It will be seen later that the colors and their small variation with phase are probably consistent with the spectroscopic data, except for the last color observation.

TABLE 1

PHOTOELECTRIC OBSERVATIONS AND TEMPERATURES

JD 2434000+	V	$P-V$	OBSERVER	T_e (° K)		T_{ion} (° K)	
				$E_{P-V}=0$	$E_{P-V}=0$ 13	Short	Long
313 89	7 41	1 05	Abt	4270	4460	4500	
336 00	5 25	0 91	Abt	4500	4710	4850	.
364 78	5 81	0 80	Abt	4710	4990	. .	4750
367 94	5 55	0 77	Abt	4750	5040	5040	..
369 90	5 63	0 732	Eggen	4800	5140	4990	..
404 85	6 33	0 96	Abt	4420	4620	4460	
419 79	5 63	0 95	Abt	4420	4670	.	4800
424 83	5 83	0 937	Eggen	4460	4670	5200	4990
460 80	5 68	1 535	Eggen	3730	3850	4580	

III. RADIAL VELOCITIES

Most of the spectrograms were obtained with the Mills spectrograph (dispersion 11 A/mm at λ 4500) attached to the 36-inch refractor; the remainder were obtained at the 36-inch with another spectrograph, giving a dispersion of 22 A/mm at λ 4500. The measured radial velocities were corrected for telescope flexure in the case of the Mills spectrograms. Table 2 gives the plate numbers, spectrograph, heliocentric times of observation, and radial velocities of the metallic absorption lines during five cycles.

The radial-velocity variation is a discontinuous one, as in the case of W Virginis (Sanford 1952). Just before each light-maximum a weak set of lines appears, displaced shortward with respect to the stronger lines. These lines quickly strengthen, move longward, and then fade during the next light-maximum (see Fig. 1). These successive sets of lines are numbered 1 through 5 in Table 2, and this numbering will be used to refer to these five cycles as well as to the corresponding five light-minima. The times of the beginning and end of each segment of the velocity-curve are sometimes uncertain because of the infrequency of the observations. The average separation of the double lines is 35 km/sec, or about 0.5 A, so at times the components of some of the strongest lines are unresolved (see Fig. 2).

The radial-velocity-curves are different for each cycle, but they have a periodicity that corresponds to the time between successive light-minima, a fact indicating that this interval is the fundamental period rather than twice this quantity. For the remainder

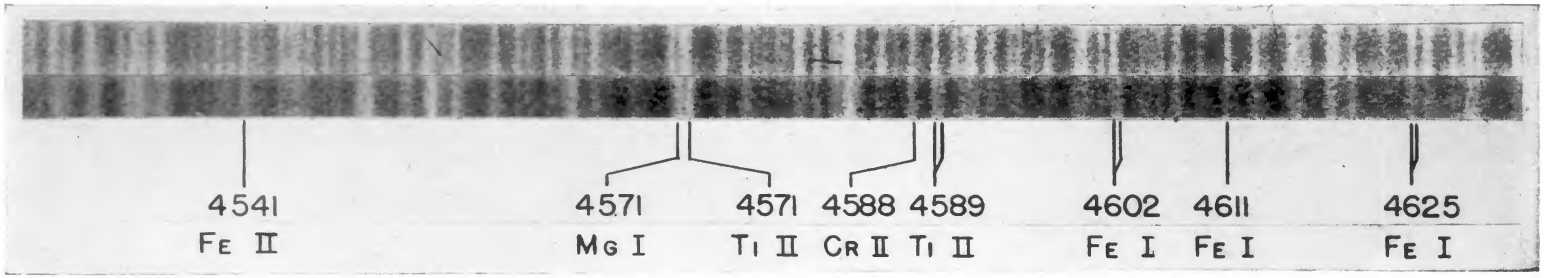

FIG. 2.—Two spectra of U Monocerotis. *Above:* with single lines (JD 2434479); *below:* with many lines doubled (JD 2434422). The shortward components of the lower spectrum have been aligned with the corresponding lines in the upper spectrum. Note that the longward component of 4602.94 *Fe* I (lower E.P. = 1.48 ev) is stronger than the shortward component, while for 4611.28 *Fe* I (lower E.P. = 3.64 ev) and for 4625.05 *Fe* I (lower E.P. = 3.23 ev) the reverse is true. This observation indicates a much higher excitation temperature for the shortward lines than for the longward.

of this paper we shall refer to the time between successive minima (about 46 days) as the period of the variable.

We wish to integrate the radial-velocity-curve to find radial displacements of the regions where the lines are formed. To perform this integration, we must know the velocity of the center of mass of the star. We cannot arbitrarily assume that the mean of the observed velocities over any time interval represents the γ-velocity, because the atmosphere may be continually expanding, as well as pulsating, or it may show an apparent systematic contraction, like solar prominences. However, we may compare the mean observed velocity with the γ-velocity if we assume that this star resembles RV Tauri stars in globular clusters. Since the peculiar motions of stars in globular clusters are probably of the order of only 5 km/sec (Wilson and Coffeen 1954), the integrated-light velocities of the clusters should closely represent the γ-velocities of individual stars in the clusters. In Table 3 we compare mean velocities of the W Virginis stars and RV Tauri stars in

TABLE 2

SPECTROSCOPIC OBSERVATIONS AND RADIAL VELOCITIES

PLATE LS	SPECTROGRAPH	HELIO JD 2434000+	RADIAL VELOCITIES (KM/SEC)				
			1	2	3	4	5
35742	III/16″	286 021	+22 6	.. ..	.. ..		.. ..
802	Mills	299 012	+30 3		. ..		.. ..
949	Mills	319 988	+61 3	.			.. .
36010..	Mills	334 028	+64 5	+29 6	.		.. .
052	Mills	339 984	+63 9	+31 3	. .		..
081	Mills	342 013	+60 5	+32 6			..
129	Mills	358 945		+44 6	. .		..
185	III/16″	369 868	.	+59 8	+19 4		.. ..
217	Mills	387 869	..	. .	+30 2		. ..
235	III/16″	393 843		..	+36 9		. .
247	III/16″	400 821			+46 9	... .	. ..
273 .	III/16″	407 898	.	..	+51 2	+20 1	.. ..
289	Mills	410 791			+51 8	.	. ..
333	Mills	422 811			+53 4	+21 8	.. ..
419	Mills	435 696			.. ..	+35 9	.. ..
425	III/16″	438 797			..	+36 3	.. ...
427	Mills	439 691			. .	+36 4	.. ....
480	Mills	459 691			.	+50 4	. ....
488	Mills	462 694			.	+53 3	+13 1
533	Mills	474 695				+56 2	+16 3
540	Mills	479 693					+23 1

clusters (Joy 1949) with the integrated-light cluster velocities (Mayall 1946). The weights W_I and W_M are those assigned by Mayall and Joy, respectively, to their velocity measures. The weight of a difference between two velocities is given by the product of the weights divided by the sum; this quantity is given in the last column of the table. Only those stars in Joy's list were used for which there were enough observations to define velocity-curves. The weighted difference of $+2 \pm 6$ km/sec between the mean velocities of the variables and the integrated-light cluster velocities shows that there is probably no significant difference between these velocities. This result was first pointed out by Joy (1949). It shows that there is no predominantly outward or inward motion of the atmospheric material in RV Tauri and W Virginis stars. We shall therefore assume that the mean observed velocity of U Monocerotis is the γ-velocity. It should be noted that a continuous velocity-curve, such as would be obtained for this star with a spectro-

graph of lower dispersion, would give the same mean velocity as that of the observed discontinuous curve.

Sanford (1933) found a variation in the mean velocity of U Monocerotis with a range of 40 km/sec and a period of about 2300 days. Our observations indicate a small decrease in mean velocity from +40.9 km/sec for cycle 2 to +37.7 km/sec for cycle 4. A comparison with Sanford's mean velocities suggests a corrected period of 2640 or possibly 1980 days. We shall adopt a mean velocity that varies linearly from +42.6 km/sec on JD 2434280 to +36.6 km/sec on JD 2434480.

The mean photographic absolute magnitude of U Monocerotis is probably of the order of −2.5 (Rosino 1951), and its mean spectral type is about G5 Ib. These values indicate a mean photospheric radius of about 65×10^6 km. We shall see later that the displacement of the reversing layer may at times be as much as 55×10^6 km or more. Normally, one would introduce a limb-darkening correction factor of about 24/17 (Getting 1934) to the radial velocities, because, when the photosphere and reversing layer are close together, the radial expansion over most of the stellar disk is not directed along the

TABLE 3

VELOCITIES OF VARIABLES IN GLOBULAR CLUSTERS

Type	NGC (M)	Integrated Vel. (Km/Sec) (Mayall)	Wt W_I	Variable No.	Mean Vel. (Km/Sec) (Joy)	Wt. W_M	Diff. (Mean − Integ.)	Weight
W Vir .	5272 (3)	−150	24	154	−153	14 0	− 3	8 84
	6218 (12)	− 32*	4	1	− 42	5 6	−10	2 33
	6254 (10)	+ 73	6	2	+ 67	7 0	− 6	3 23
RV Tau .	5904 (5)	+ 45	13	42	+ 54	8 0	+ 9	4 95
	5904 (5)	+ 45	13	84	+ 50	8 0	+ 5	4 95
	6779 (56)	−154	5	6	−132	7 7	+22	3 03
	7089 (2)	− 3	17	11	− 4	10 8	− 1	6 60
Weighted mean	.		...			.	+ 2±6	..

* This is a revised unpublished velocity determined by Dr. N U Mayall, to whom the author is grateful for this information

line of sight. In view of the possible large separation of the photosphere and reversing layer, this factor will not be used in this case. Our displacements may therefore be conservative.

The displacements, $r - r_n$, from an arbitrary radius, r_n, can now be calculated for each cycle, n. The discontinuity of the velocity-curve indicates that we observe different material during successive cycles, and therefore the radial velocities give no information on the relative locations of successive segments of the displacement-curve, i.e., on the relative values of the r_n's. In illustrating the displacements in Figure 1, we have arbitrarily given each cycle the same maximum displacement. This procedure probably does not represent the actual situation.

In Table 4 are tabulated the ranges in visual light and displacement and the initial outward velocity (γ-velocity *minus* initial observed velocity) for each of five cycles. All three quantities are directly correlated, a fact indicating (1) that deep light-minima are associated with large expansions, while shallow ones occur during small expansions, and (2) that regions of line formation starting with large outward velocities move to large displacements. The minima in visual light occur about 10 days after maximum expansions of the atmosphere. The first correlation, which was first pointed out for several RV Tauri stars by Sanford (1931) and by McLaughlin (1938, 1941), is such that each

27×10^6-km range in displacement corresponds to a decrease in visual light by 1 mag. This result is only very approximate, since the duration of the segments of the velocity-curve and hence the ranges in displacement depend in part on the frequency of the observations. Since we did not observe the beginning of cycle 1, the initial outward velocity may have been larger than 19.9 km/sec. Our small amount of data indicates that the displacement ranges depend more on the duration of a set of lines than on the velocity ranges (or initial outward velocities) of the lines.

IV. SPECTROPHOTOMETRY

In the following discussion our line intensities have been compared with those computed for a normal stellar atmosphere. Since an atmosphere with two regions of line formation is not normal, the results must be regarded with caution. The only justification for our approach is that, at the outset, we have very little knowledge as to what kind of model actually represents the star. We hope that these preliminary results will be of

TABLE 4

LIGHT, DISPLACEMENT, AND VELOCITY RANGES

Cycle No.	Visual-Light Range (Mag.)	Displacement Range	Initial Outward Velocity (Km/Sec)	Cycle No.	Visual-Light Range (Mag.)	Displacement Range	Initial Outward Velocity (Km/Sec)
1.	2 1	56×10^6km	19 9+	4	1 1	36×10^6km	18 9
2	0 4	12	11 5	5 .	1 7+	.. .. .	23 9
3 .	1 2	27	20 5				

aid in deciding between models and that the basic data may then be used to test the models. We see no a priori reason for doubting the results obtained during times of single lines, but when the lines are double, continuous opacities associated with the two-line spectra may affect the observed line intensities. The size of the corrections for this effect cannot be determined with the information available, i.e., the total opacities and relative locations of the two regions of line formation are not known. It is significant that reasonable values of the physical parameters have been derived at these times without applying any corrections. Within the completeness of our measures in this star, as well as in W Virginis, we have found no evidence for dilution of radiation (except in the zero-volt *Fe* I lines), stratification, or departures from local thermodynamic equilibrium (except for large differences between ionization and excitation temperatures, a result which is also often obtained in nonvariable stars). All the *Fe* absorption-line intensities (except for the zero-volt lines) are those to be expected, within our accuracy of measurement, from a specification of the abundances, excitation temperature, ionization temperature, continuous opacity, turbulent velocity, and damping constant for each set of lines present. We shall not discuss the *TiO* bands present at deep light-minima or the *H* emission lines observed during increasing light.

Equivalent widths for lines of *Fe* I and *Fe* II were measured on the fifteen Mills and on two of the III/16″ plates. The method of reduction is essentially that described for W Virginis (Abt 1954). To compare measures on the III/16″ plates with those on the Mills plates, we made a comparison of two plates of α Persei taken with these two spectrographs. It was found that on the lower-dispersion spectrograms the lines were measured 15 per cent shallower and wider than on the higher-dispersion plates, so that equivalent widths are 12 ± 12(p.e.) per cent larger. Corrections of this amount were applied to the III/16″ measures. A comparison of the Mills equivalent widths for α Persei with

those determined by Greenstein (1948) showed the former to be 17 ± 12(p.e.) per cent smaller. Table 5 gives the equivalent widths, W, expressed as $-\log W/\lambda$. For plates with double lines, separate columns are used for the shortward and longward components. For the III/16″ plates the corrected values are given. The f-values used are those given in the paper on W Virginis; these were taken from laboratory, solar, and stellar sources.

The empirical curves of growth were compared with theoretical ones (Wrubel 1949) for a Milne-Eddington model atmosphere. Some justification will be given later for the use of this model rather than a Schuster-Schwarzschild model. The results are tabulated in Table 6, whose first two columns give the plate number and the component measured. Column 3 gives the number of lines measured. These numbers are small because of the very limited spectral range available; there were just barely enough lines to construct curves of growth. However, this spectral range ($H\gamma$ to λ 4650) is one in which the lines are almost entirely free of blends. The double lines are generally not completely separated, but the observed changes in line strengths are so large that useful results can nevertheless be obtained. The damping parameter, a, cannot be determined when all the lines are weak: assumed values for these times are followed by a colon in column 4 of Table 6.

The variation in Doppler velocity, V, is given in column 5 and is shown in Figure 3. This velocity increases during each expansion and during the subsequent contraction from an initial value of about 3 to about 7 km/sec. The accuracy of measurement is about ±1 km/sec on each plate. The velocities are too large to be due to thermal motion; they may be due either to some form of turbulent motion or to a dispersion in the pulsation velocity.

The excitation temperatures, T_{ex}, are also shown in Figure 3. Their behavior from cycle to cycle is irregular, perhaps due in part to the low precision of ±500° of their determination. At times of double lines the shortward component always seems to have the higher excitation temperature. At times of large displacement the zero-volt *Fe* I lines do not fit the curve of growth chosen for the 1.5 to 3.5 ev lines, and consequently for these times the zero-volt lines were not used in the determination of T_{ex}. The reason for this discrepancy will be considered in the discussion of R Scuti, for which we have better material in this regard.

In the absence of absolute f-values for *Fe* II, we converted the line strengths of *Fe* I and *Fe* II to abundances relative to those in α Persei. From the degree of ionization of *Fe* I in α Persei (Greenstein 1948) we then derived the degree of ionization in U Monocerotis. Columns 7 and 8 in Table 6 give the logarithms of the relative apparent abundances, N/κ, in U Monocerotis compared to α Persei for *Fe* I and *Fe* II, respectively. Column 9 gives the degree of ionization of *Fe* I. These numbers are plotted in Figure 4, where the abundances marked with a vertical line (and by a colon in Table 6) are uncertain; they were derived from incomplete curves of growth that depend on assumed values of a, V, and T_{ex}. Those marked with an arrow in Figure 4 and an inequality in Table 6 are maximum values obtained from an absence of that component.

V. DISCUSSION

A striking feature of Figure 4 is that, although the apparent abundances are observed to vary by a factor of more than 1000, the corresponding degrees of ionization are nearly constant; at only one time does the degree of ionization differ from the mean by more than a factor of 2. The degree of ionization is a function of the ionization temperature (T_{ion}), electron pressure (P_e), and—for a detached shell—the dilution factor. The *Fe* I lines show no dilution effects (except in the zero-volt lines) in the sense of intensity differences for lines originating from metastable and stable levels. Therefore, it appears that P_e (which varies over a range of 10^3) and T_{ion} vary in such a manner that the ionization of *Fe* I is constant.

At this point we shall consider the possible reasons for time variations in the apparent

TABLE 5

VALUES OF $-\log W/\lambda$

λ	Element	Multiplet No.	Plate No. and Component											
			35742	35802	35949	36010		36052		36081		36129	36185	
						Short	Long	Short	Long	Short	Long		Short	Long
4389.24	*Fe* I	2										4.03		
4404.75	*Fe* I	41	3 77			3.98	4.10	3.84		3.90	4.13	3 77	3.90	
16.82	*Fe* II	27				4.42		4.22		4.32		4.19		
27.31	*Fe* I	2	3.85		3 79			3 76		4.03	4.08	3.88		
32.57	*Fe* I	797												
47.72	*Fe* I	68	4.27	4.17	4.14	4.26		4.18				4.19	4.57	5 16
72.92	*Fe* II	37	4.18	3.98	4.36	4.36		4.20		4.21		4.23	4.52	
76.02	*Fe* I	350	4.31	4.14	4.25			4.16		4.16		4.20	4.40	5 04
84.23	*Fe* I	828	4.20		4.25	4.25		4.19		4.39		4.31	4.47	
85.68	*Fe* I	830				4.55								
89.18	*Fe* II	37						4.18		4.15		4.22		
89.74	*Fe* I	2	4.03	3 79	3.91							3.98	4.30	
91.40	*Fe* II	37	4.30	4.16	4.37	4.27	4.69	4.23		4.20		4.28	4.38	
94.57	*Fe* I	68	4.11	3.94	4.16					4.16	4.20	4.01		
4504.84	*Fe* I	555	4.89	4.42				4.98		4.88				
08.28	*Fe* II	38	4.17	4.19	4.23	4.24	4.48	4.25	4.74	4.20	4.62	4.21	4.23	
15.34	*Fe* II	37	4.13	4.12	4.23	4.24	4.47	4.21		4.18	4.76	4.15	4.29	4.77
20.23	*Fe* II	37	4.09	4.05	4.26	4.24	4.66	4.24		4.21		4.08		
22.63	*Fe* II	38	4.02	3.80	4.13	4.05	4.27	4.02	4.36	4.02	4.45	4.03	4.20	
28.62	*Fe* I	68	4.08	3.86	4.14							3.99	4.24	4.31
41.52	*Fe* II	38	4.31	4.09	4.30	4.30	4.72	4.26	4.84	4.25		4.20	4.50	4.77
76.33	*Fe* II	38	4.37	4.20		4.39	4.69	4.30	4.70	4.37		4.25	4.60	4.88
82.83	*Fe* II	37	4.37			4.39		4.32		4.29				
83.83	*Fe* II	38	4.07	4.04	4.05	3.97	4.30	3.99	4.75	4.08		3.97		
87.13	*Fe* I	795	4.99	4.38				4.93		5.22		5 09		
4602.00	*Fe* I	39	4.61	4.20	4.41			4.56		4.71		4.56		
02.94	*Fe* I	39	4.30	4.09	4.26	4.27	4.46	4.22		4.29		4.15	4.93	
11.28	*Fe* I	826	4.54	4.19	4.50	4.68	5 04	4.44		4.51		4.38		
20.51	*Fe* II	38	4.46	4.27	4.71	4.43		4.42		4.42		4.42	4.55	5 16
25.05	*Fe* I	554	4.54	4.28	4.48	4.44		4.47		4.41		4.50	4.83	
32.92	*Fe* I	39	4.49	4.17				4.68		4.32		4.39		
43.47	*Fe* I	820		4.23						4.69		4.66		
47.44	*Fe* I	409	4.41	4.14		4.40				4.29		4.42		

TABLE 5—*Continued*

λ	Element	Multiplet No.	Plate No. and Component												
			36217	36289		36333		36419	36427	36480	36488		36533		36540
				Short	Long	Short	Long				Short	Long	Short	Long	
4389.24	*Fe* I	2	3.94		3.93		3.93	4.18	4.09	4.02		4.20			
4404.75	*Fe* I	41	3.72		3.77		3.88	3.84	3.80	3.81		3.91	3.91	4.11	3 69
16.82	*Fe* II	27							4.22				4.16		4.17
27.31	*Fe* I	2	3.83		3.84		3.91	3.94	3.88	3.90		3.93	4.06	4.25	4.02
32.57	*Fe* I	797	4.54		4.90		3.91								
47 72	*Fe* I	68	4.22		4.22	4.44	4.36			4.17		4.30	4.22		4.16
72.92	*Fe* II	37	4.10		4.27	4.30		4.27	4.24	4.23		4.34	4.08		4.10
76.02	*Fe* I	350	4.23		4.18	4.41	4.49	4.33	4.32	4.20		4.36	4.15		4.15
84.23	*Fe* I	828	4.09			4.41		4.43	4.28			4.63			4.05
85.68	*Fe* I	830													
89.18	*Fe* II	37													
89 74	*Fe* I	2	3.87		3.89		4.00	4.03	4.00	3.98		4.06			
91.40	*Fe* II	37	4.24			4.24	4.96	4.27	4.24	4.23			4.07		4.15
94.57	*Fe* I	68	4.02		4.04	4.13	4.29	4.12	4.04	4.05		4.15	4.22		3.94
4504.84	*Fe* I	555	4.50		5.47	5.03						5.00			4.58
08.28	*Fe* II	38	4.15	4.76	4.20	4.15	4.36	4.18	4.15	4.20	4.76	4.16	4.31		4.21
15.34	*Fe* II	37	4.18	4.73	4.16	4.23	4.39	4.20	4.16	4.20	4.63	4.26	4.22		4.08
20.23	*Fe* II	37	4.12	4.65	4.19	4.22	4.64	4.16	4.16	4.17		4.16	4.21		4.04
22.63	*Fe* II	38	3.91	4.61	3.95	4.05	4.21	4.00	3.93	3.98	4.43	4.13			3.88
28.62	*Fe* I	68	4.04		3.95			4.00	4.04	4.03		4.04			3.99
41.52	*Fe* II	38	4.18		4.21	4.15		4.32	4.22	4.30		4.36			4.18
76.33	*Fe* II	38	4.30		4.23	4.37	4.59	4.33	4.33	4.34			4.39		4.23
82.83	*Fe* II	37	4.16					4.33	4.27		4.66	4.34	4.17		4.18
83.83	*Fe* II	38	4.00		3.96	3.95		3.99	4.04	4.01	4.50	4.08	3.98		3.90
87.13	*Fe* I	795	4.58		5.00				4.99			5.26			4.69
4602.00	*Fe* I	39	4.34		4.45			4.74	4.61	4.49		4.66	4.36		4.28
02.94	*Fe* I	39	4.23		4.17	4.51	4.34		4.22	4.16		4.31	4.23		4.13
11.28	*Fe* I	826	4.23			4.56		4.52	4.42	4.42		4.63	4.38		4.23
20.51	*Fe* II	38	4.34		4.37	4.45		4.52	4.36	4.45			4.35		4.32
25.05	*Fe* I	554	4.32		4.45	4.48	4.83	4.56	4.47	4.46			4.35		4.28
32.92	*Fe* I	39	4.20		4.27	4.64	4.56	4.46	4.40	4.30		4.59	4.35		4.12
43.47	*Fe* I	820	4.33		4.70	4.76		4.75	4.50	4.84		5.15	4.58		4.31
47 44	*Fe* I	409	4.24		4.20	4.42	4.53	4.40	4.24	4.43			4.24		4.12

TABLE 6

SPECTROPHOTOMETRIC RESULTS

Plate LS (1)	Component (2)	n (3)	log a (4)	V (Km/Sec) (5)	T_{ex} (6)	log $[(N'/\kappa)_v/(N'/\kappa)_a]$ (7)	log $[(N''/\kappa)_v/(N''/\kappa)_a]$ (8)	log (N''/N') (9)	log $\bar{\kappa}$ (10)	T_{ion} (11)	log P_e (12)	log P (13)	log ρ (14)	log g_e (15)
35742		27	−1.8	3.2	3650	+1.65	+1.45	+2.76	−3.34	4540	−2.29	+1.54	− 9 73	−1.50
35802		25	−3.0	4.0	3850	+2.98	+2.18	+2.16	−4.07	3910	−3.29	+0.90	−10.31	−2.87
35949	Long	20	−3 0	6.8	3500	+1.25	+0.62	+2.33	−2.51	4800	−1.38	+2.47	− 8.83	+0.26
	Short	0	.. ..	.. .	. .	. .	<−2.64	. . .	.. .	.. .	...	.	. ..	.. . .
36010	Long	11	−2.6:	6.2	3630	+0.20	−0.18	+2.58	−1.71	5540	−0.39	+2.63	− 8.73	+1.22
	Short	20	−2.2	3.8	6000	+0.50	−0 02	+2.44	−2.64	4750	−1.52	+2.33	− 8.96	−0.01
36052	Long	5	. .	.	.	..	−0.63:	. .	.. .	. .	..	.	.	.
	Short	25	−2.2	5.5	4420	+0.93	+0.36	+2.39	−2.25	4850	−1.04	+2.91	− 8.39	+0.96
36081	Long	6	. .	. .	.	. .	−0.68:	. .	...	. .	..	...	.	.
	Short	27	−2.2	5.6	4200	+0.99	+0.53	+2.50	−2.42	4940	−1.23	+2.44	− 8.87	+0.32
36129	Long	27	−2.2	7.2	3650	+1.27	+0.80	+2.49	−2.69	4800	−1.55	+2.20	− 9.10	−0.19
	Short	0	.. ..	..	.	. .	<−2.64	. .		...	..	. .	.	.
36185	Long	7	..	. .	.	.	−0.36:				.	.	.	.
	Short	17	−2.2:	4.3	3730	+0.89	+0.64	+2.71	−2.53	4990	−1.35	+2.12	− 9.20	−0.11
36217	.	27	−2.6	3.6	4340	+2.14	+1.58	+2.40	−3 47	4310	−2.52	+1.56	− 9 69	−1.61
36289	Long	27	−2.2	5.8	3480	+1.71	+1.42	+2.67	−3.31	4500	−2.28	+1.63	− 9 64	−1.38
	Short	4	..		. .	. . .	−1.87:	. . .	. . .	. .	..			
36333	Long	17	−2.2:	10.0	3050	+1.02	+0 43	+2.37	−2.32	4940	−1.14	+2.59	− 8.72	+0.57
	Short	21	−2.2	3.0	5480	+0.31	+0.58	+3.23	−2.47	5250	−1.44	+1.29	−10.05	−0.88
36419		25	−1.8	5.0	3790	+1.17	+0.93	+2.72	−2.82	4850	−1.69	+1.85	− 9 45	−0.67
36427	.	28	−1.8	5.2	3850	+1.21	+0.93	+2.68	−2.82	4800	−1.70	+1.95	− 9.35	−0.57
36480		25	−2.2	5.8	3500	+1.58	+1.15	+2.53	−3.04	4580	−1.97	+1.95	− 9.33	−0 79
36488	Long	25	−2.2	5.5	3360	+1.48	+1.27	+2.75	−3.16	4670	−2.09	+1.59	− 9 70	−1.27
	Short	5	..	. .	. .	..	−0.88:		..	.		.	..	..
36533	Long	2	.. .	.	...	. .	−2.09:	.	...	.	. .	.	. .	
	Short	22	−2.6	4.6	4000	+1.53	+1.36	+2.79	−3.25	4620	−2.18	+1.54	− 9 74	−1.41
36540	.	28	−2.6	4.6	4380	+1.83	+1.47	+2.60	−3.36	4460	−2.35	+1.60	− 9 67	−1.46

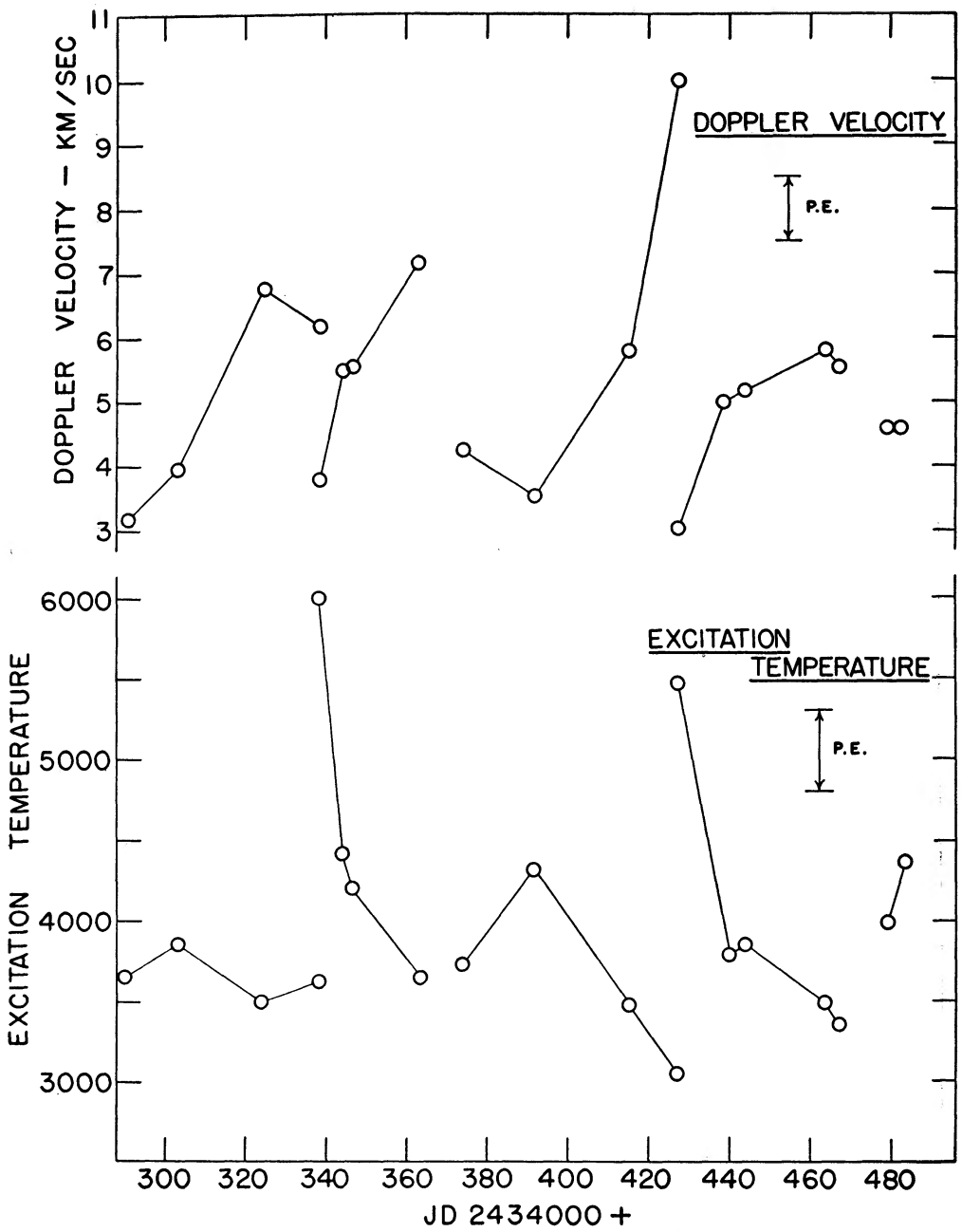

FIG. 3.—*Top:* Doppler velocities; *bottom:* excitation temperatures. The two vertical lines indicate the estimated probable errors in these quantities.

abundances, particularly during times when the lines are single. It will be shown below that at least 99 per cent of the *Fe* atoms are in the form of *Fe* II. Therefore, the *Fe* II abundance-curve gives the variation in *Fe* abundance under conditions of local thermodynamic equilibrium. We see in Figure 4 that, as an extreme case, during cycle 1 the apparent abundance decreased by a factor of 36 between the second and third observations. This change is very apparent in the line strengths on the two spectrograms, both of which had single lines. We now consider four causes for apparent abundance changes.

1. *Variation in surface density.*—If the observations had been reduced with curves of growth for a Schuster-Schwarzschild model, we would have derived values of $\mathfrak{N}H$, the number of *Fe* atoms per square centimeter above the photosphere. These values would have been proportional to the values of N/κ of the Milne-Eddington model. In the case of a transparent expanding shell, $\mathfrak{N}H$ would change because the surface density varies inversely as the square of the radius of the shell. However, for the two spectra mentioned earlier, the abundance per square centimeter decreased as the mean radius of the region of line formation decreased 8.5×10^6 km, i.e., the change in surface density would produce the opposite effect from that observed.

2. *Excess of far-ultraviolet radiation.*—The abundance of *Fe* in U Monocerotis as derived from lines of *Fe* I and *Fe* II could vary through ionization to *Fe* III from an excess of radiation in the vicinity of λ 767, which corresponds to the ionization potential of *Fe* II. The general weakening of all the absorption lines between the times mentioned is not consistent with such selective effects, which depend on a comparison of the ionization potential of each element with the wave-length profile of the proposed ultraviolet excess.

3. *Nonspherically symmetric models.*—Various models (e.g., large filaments, nonspherically symmetric shells, rings, satellites, and spots) can be proposed in which the amount of material projected in front of the disk varies with time. If these are to produce abundance changes by a factor of 36 or more, they are likely to cause significant changes or scatter in the variations in velocity, light, and other quantities. We should not postulate complicated or nonspherically symmetric models unless they are suggested by more than one parameter.

4. *Variable continuous opacity.*—The variation in apparent abundance, N/κ, may be due to a variation in the continuous opacity, κ, in the region where the lines are formed. It will be seen that numerical values of κ then lead to ionization temperatures that are probably in agreement with effective temperatures derived from colors and from spectral types. If the continuous opacity is sufficiently large at most, or all, times to obscure part of the region of line formation, this region as a whole must be opaque in the continuum, i.e., the photosphere is located within this region. In view of our dissatisfaction with the first three causes, we shall provisionally accept this explanation and investigate its consequences. One of these is that a Milne-Eddington model gives a more useful representation of the atmosphere than does a Schuster-Schwarzschild model. We therefore no longer accept those estimates, based on a Schuster-Schwarzschild model, of the thickness of the regions of line formation in W Virginis (Abt 1954).

The curves of growth for *Fe* II yield the quantity

$$\log \frac{[N(Fe\ \text{II})/\kappa]_U}{[N(Fe\ \text{II})/\kappa]_a}.$$

From the degree of ionization in Figure 4, $N(Fe\ \text{I}) < 10^{-2}\ N(Fe\ \text{II})$. With sufficient accuracy, the Saha equation gives

$$\log \frac{N(Fe\ \text{III})}{N(Fe\ \text{II})} - \log \frac{N(Fe\ \text{II})}{N(Fe\ \text{I})} = -\frac{5040}{T_{\text{ion}}}\left[I(Fe\ \text{II}) - I(Fe\ \text{I})\right] = -\frac{41{,}800}{T_{\text{ion}}}, \quad (1)$$

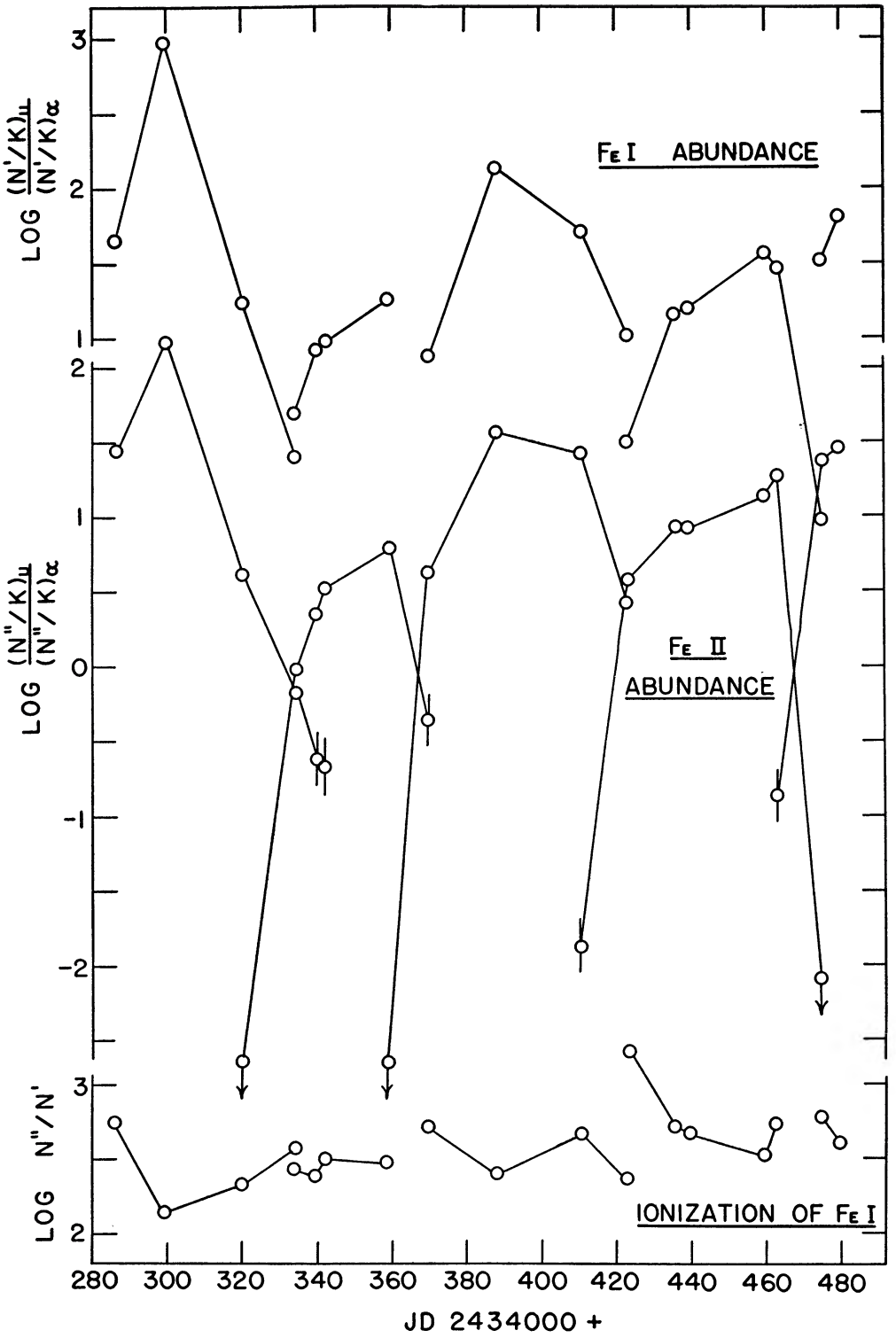

FIG. 4.—*Top and center:* apparent abundances of *Fe* I and *Fe* II, respectively, relative to those in α Persei; *bottom:* the degree of ionization of *Fe* I in U Monocerotis.

where I is the ionization potential. For temperatures of 5500° or less, $N(Fe\ \text{III}) < 10^{-4}\ N(Fe\ \text{II})$. Therefore, with 1 per cent accuracy, $N(Fe) = N(Fe\ \text{II})$. If we assume the same fraction of *Fe* per gram of material in U Monocerotis as in α Persei, we obtain

$$\frac{N(Fe)_U}{N(Fe)_\alpha} = \frac{N(Fe\ \text{II})_U}{N(Fe\ \text{II})_\alpha} = 1. \tag{2}$$

Therefore,

$$\frac{[N(Fe\ \text{II})/\kappa]_U}{[N(Fe\ \text{II})/\kappa]_\alpha} = \frac{\kappa_\alpha}{\kappa_U}. \tag{3}$$

The relation between κ and the mean opacity, $\bar{\kappa}$, is given by Chandrasekhar and Münch (1946). Knowing $\bar{\kappa}$ for α Persei (Greenstein 1948), we derive the values of $\bar{\kappa}$ for U Monocerotis that are given in column 10 of Table 6.

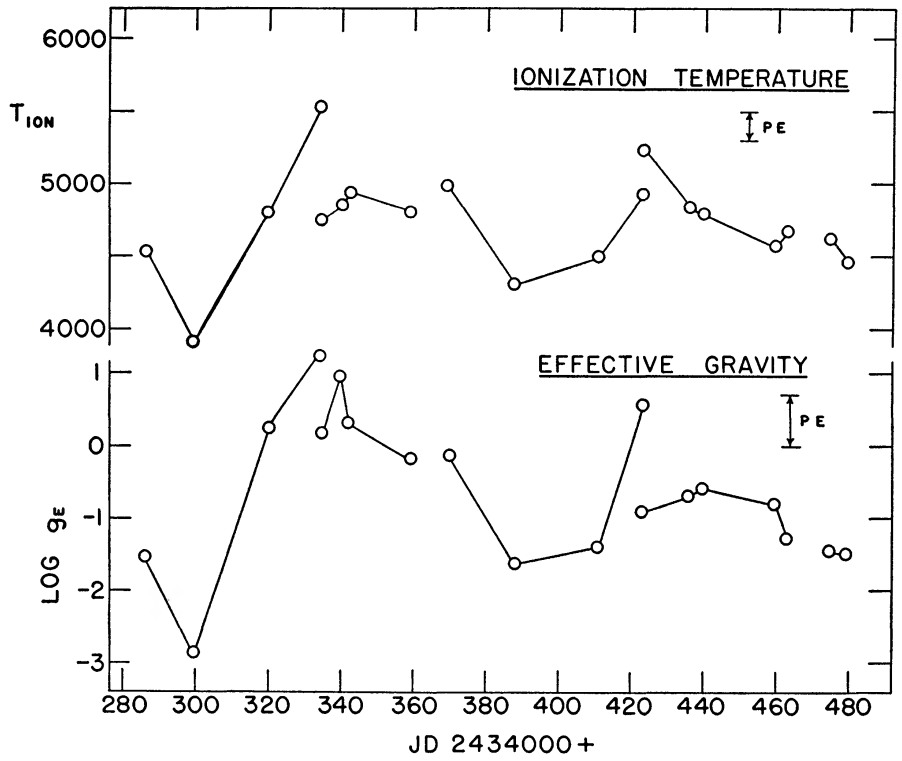

FIG 5.—*Top:* ionization temperatures; *bottom:* effective gravity determined spectroscopically. The two vertical lines represent the estimated probable errors in these quantities

The continuous opacity is a function of T_{ion} and P_e (Chandrasekhar and Münch 1946). Similarly, the degree of ionization is a function of these two quantities. For each time of observation, we solved simultaneously for T_{ion} and P_e (in dynes per square centimeter), with the results given in columns 11 and 12 of Table 6. The variation in T_{ion} is shown in Figure 5. The size of the probable errors in the determination of $\bar{\kappa}$, T_{ion}, and P_e cannot be estimated accurately, but a rough check is obtained by comparing results on four pairs of plates for which the time interval between plates is only 3–5 days. The mean differences are ± 0.10 in log $\bar{\kappa}$, $\pm 100°$ in T_{ion}, and ± 0.12 in log P_e. We shall assume probable errors (p.e.) per observation of twice these amounts.

We can now compare the ionization temperatures in the regions where the lines are

formed with the effective temperatures derived from the colors in Table 1. From Eggen's work (1951*a*, *b*) we have the relation between $P - V$ and spectral type for unreddened I*b* supergiants. Keenan and Morgan (1951) give the relation between spectral type and effective temperature, T_e, for population I stars. Table 1 gives the effective temperatures for no interstellar reddening (color excess $E_{P-V} = 0$) and the interpolated values of T_{ion} for one or more components. The ionization temperatures are systematically higher by 260°. However, if we assume that the star has a color excess of 0.13 mag., this systematic difference disappears, and the temperatures agree (except for the last one), with a probable error of $\pm 120°$. Stebbins and Huffer (1934) predict a color excess on the C_1 scale of 0.07 mag. for the galactic longitude (194°) and distance (about 500 parsecs) of this star. Since our color system more nearly resembles the (B, V) system of Johnson and Morgan (1951), the predicted color excess is of the order of 0.14 mag. (Morgan, Harris, and Johnson 1953), if we may extrapolate from their correlations for B-type stars. Therefore, our assumed color excess is of reasonable size. Rosino (1951) estimated the spectral-type range of U Monocerotis to be F8e I*b* to K0p I*b*, for which we would expect (Keenan and Morgan 1951) a range in effective temperature of 5300°–3820°. Our ionization temperatures range from 5540° to 3910°. We conclude that the ionization temperatures computed on the basis of a variable continuous opacity are probably in agreement with the observed spectral types and with the effective temperatures derived from the colors. It should be noted that if $\bar{\kappa}$ were constant, computed values of T_{ion} and of P_e would be nearly constant at all times, since the degree of ionization of *Fe* I shows very little variation.

There are often very large differences (as much as 1900°) between the excitation and ionization temperatures (see Fig. 2). In the spectra the intensity ratios of low- to high-excitation lines give a later spectral type than comparisons of lines from two stages of ionization. For this reason the spectra often are not similar to any standards for spectral classification.

We are now ready to discuss the variation of T_{ion} and P_e with displacement, $r - r_n$, during the course of each cycle. Within the probable errors in T_{ion} and P_e, these quantities decrease during each expansion and increase during the subsequent contraction. However, the values of T_{ion} and P_e at the times of double lines may be only rough approximations, because in the case of the Milne-Eddington model the observed line intensities must be corrected for the composite nature of the spectrum. The variations in T_{ion} and log P_e with time are rather similar in shape, a consequence of the relative constancy of the degree of ionization of *Fe* I.

During each cycle the shapes of the variation in T_{ion} (Fig. 5) and in log P_e are very similar to the corresponding segments of the displacement-curves (Fig. 1). For the two cycles (1 and 3) for which our data extend over large ranges in displacement, the correlations are given roughly by

$$\frac{\Delta T_{\text{ion}}}{\Delta (r - r_n)} = -3.^{\circ}0 \times 10^{-10}\ \text{cm}^{-1}, \tag{4}$$

$$\frac{\Delta \log P_e}{\Delta (r - r_n)} = -5.7 \times 10^{-13}\ \text{cm}^{-1}. \tag{5}$$

We find that with a scatter (computed as a probable error) of $\pm 150°$ in T_{ion} and ± 0.24 in log P_e, equations (4) and (5) hold for all five cycles. This scatter is about the same as the estimated probable errors in the determination of T_{ion} ($\pm 200°$) and log P_e (± 0.24). Therefore, as a rough approximation, the rates of change of temperature and of electron pressure with displacement are the same for all cycles and are numerically the same during expansion as during contraction.

If our values of T_{ion} and P_e have a meaning in the sense that they represent mean conditions in a region that is relatively homogeneous, we may derive the total pressures and densities in the region. The metals are singly ionized, but hydrogen is only slightly ionized. With 1 per cent accuracy, we may write

$$\frac{P_e}{P} = x_H + \frac{1}{A}, \tag{6}$$

where P is the total gas pressure, x_H is the degree of ionization of H, and A is the hydrogen-to-metal ratio. Assuming $A = 10^{4\,2}$, we obtain the total pressures, and from the perfect gas law we derive densities, ρ. These quantities are given in columns 13 and 14 of Table 6. The equation of hydrostatic equilibrium is

$$\frac{dP}{d\tau} = \frac{g}{\bar{\kappa}(\tau)}. \tag{7}$$

We shall assume a pressure gradient of this form to obtain a spectroscopically determined effective acceleration, g_e. With sufficient accuracy, it may be shown (Greenstein 1948) that

$$g_e = \frac{P(\tau_0)\ \bar{\kappa}(\tau_0)}{2\tau_0}, \tag{8}$$

where P and $\bar{\kappa}$ are evaluated at the mean optical depth of line formation, τ_0, which we assume to be 0.25. Resulting values of log g_e are given in column 15 of Table 6 and are plotted in Figure 5. It is probably significant that the g_e's are small at maximum expansions (compare with displacements in Fig. 1) and large at contractions. In fact, the variation in g_e could be used to relate the segments of the displacement-curve if we could believe that the g_e's are directly related to the gravitational g's, whose mean value is of the order of $10^{1\,4}$. The range of 10^4 in g_e is much larger than the expected range in g.

We shall not discuss at length the question of what kind of model best fits the observations. As in the case of W Virginis, the observations suggest, at first glance, spherical layers that expand and contract in a time interval greater than that of the ejection of these layers, with successive ones meeting one another. The observed Doppler velocity dispersion is too small if the layers are to fill in the regions between them. However, the problem of the interpenetration of layers is a formidable one. It may perhaps be avoided if the layers are assumed to be nonhomogeneous and to consist of many condensations. This assumption would then lead to the question of how such a layer can be optically thick. It may be that more detailed calculations on the behavior of shock waves in stellar atmospheres will lead to an acceptable model.

One final matter requires discussion, although the relevant data are meager. The colors show very little variation, except for the final measure. For example, the first two observations in Table 1 were taken during a deep light-minimum and the succeeding maximum, but the color difference is only 0.14 mag. Since the light and displacement variations are nearly 180° out of phase (light-minima near maximum expansions), the light-changes must be due predominantly to changes in surface brightness. The color variation is insufficient to account for the light-variation. If the region of line formation is opaque, the photosphere lies in that region, and the light-variation should depend on the area and temperature of the region. Additional photoelectric data are needed, although these would be most meaningful if obtained simultaneously with spectra.

I am grateful to Dr. O. J. Eggen for his photoelectric observations, to the A.A.V.S.O. for the visual observations, and to Drs. J. L. Greenstein, G. H. Herbig, and W. P. Bidelman for reading the manuscript and making helpful suggestions

REFERENCES

Abt, H. A. 1954, *Ap. J.*, suppl , **1,** 63 (No 3).
Chandrasekhar, S., and Münch, G. 1946, *Ap. J.*, **104,** 446.
Eggen, O. J. 1951*a*, *Ap. J.*, **113,** 367; *Lick Obs. Contr.*, Ser II, No. 32.
———. 1951*b*, *Ap. J.*, **114,** 141; *Lick Obs. Contr.*, Ser. II, No. 37.
Getting, I A. 1934, *M.N.*, **95,** 139.
Greenstein, J. L. 1948, *Ap. J.*, **107,** 151; *McDonald Contr.*, No 145.
Johnson, H. L , and Morgan, W. W. 1951, *Ap. J.*, **114,** 522; *McDonald Contr.*, No 205.
Joy, A. H. 1949, *Ap. J.*, **110,** 105.
———. 1952, *ibid.*, **115,** 25.
Keenan, P. C., and Morgan, W. W. 1951, *Astrophysics*, ed. J. A. Hynek (New York: McGraw-Hill Book Co.), chap. 1.
McLaughlin, D. B. 1938, *Pub. Univ. Michigan Obs.*, **7,** 57.
——— 1941, *Ap. J.*, **94,** 94.
Mayall, N. U 1946, *Ap. J.*, **104,** 290; *Lick Obs. Contr* , Ser II, No 15.
Morgan, W. W., Harris, D. L , and Johnson, H. L. 1953, *Ap. J.*, **118,** 92; *McDonald Contr.*, No. 224.
Rosino, L. 1951, *Ap. J.*, **113,** 60.
Sanford, R. F. 1931, *Ap. J.*, **73,** 364; *Mt. W. Contr.*, No. 424.
———. 1933, *Ap. J.*, **77,** 120; *Mt. W. Contr.*, No. 465.
———. 1952, *Ap. J.*, **116,** 331.
Stebbins, J , and Huffer, C. M. 1934, *Pub. Washburn Obs* , Vol **15,** Part 5.
Wilson, O. C., and Coffeen, M. F. 1954, *Ap. J.*, **119,** 197.
Wrubel, M. H. 1949, *Ap. J.*, **109,** 66.